

FRAME: Pre-Training Video Feature Representations via Anticipation and Memory

Sethuraman T V^{1,2}, Savya Khosla², Vignesh Srinivasakumar^{2†}, Jiahui Huang¹, Seoung Wug Oh¹,
Simon Jenni¹, Derek Hoiem², Joon-Young Lee¹

¹Adobe Research, ²University of Illinois Urbana-Champaign

[†]Now at NVIDIA

Project: <https://video-frame-encoder.github.io/vid-frame-encoder/>

Abstract

Dense video prediction tasks, such as object tracking and semantic segmentation, require video encoders that generate temporally consistent, spatially dense features for every frame. However, existing approaches fall short: image encoders like DINO or CLIP lack temporal awareness, while video models such as VideoMAE underperform compared to image encoders on dense prediction tasks. We address this gap with FRAME, a self-supervised video frame encoder tailored for dense video understanding. FRAME learns to predict current and future DINO patch features from past and present RGB frames, leading to spatially precise and temporally coherent representations. To our knowledge, FRAME is the first video encoder to leverage image-based models for dense prediction while outperforming them on tasks requiring fine-grained visual correspondence. As an auxiliary capability, FRAME aligns its class token with CLIP’s semantic space, supporting language-driven tasks such as video classification. We evaluate FRAME across *six dense prediction tasks on seven datasets*, where it consistently outperforms image encoders and existing self-supervised video models. Despite its versatility, FRAME maintains a compact architecture suitable for a range of downstream applications.

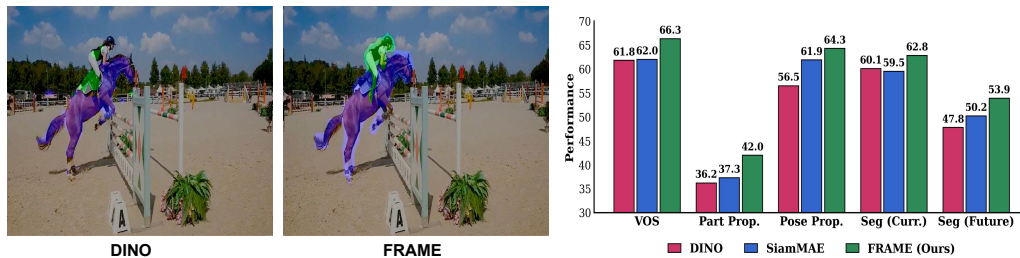


Figure 1: FRAME outperforms state-of-the-art self-supervised models (DINO, SiamMAE) on multiple dense video tasks. The student (FRAME) surpasses the teacher (DINO) by learning to predict current and future features using memory, improving temporal consistency and visual correspondence. (Right) Eg: VOS where FRAME improves segmentation of horse and rider. (left) Tasks shown: VOS = Video Object Segmentation [33], Part Prop. = Part Propagation [59], Pose Prop. = Pose Propagation [22], Seg = Semantic Segmentation [3] of current & future frame.

1 Introduction

Our goal is to build a versatile **self-supervised video frame encoder for dense prediction tasks**. While self-supervised learning has achieved strong results in static image understanding and some

video understanding tasks, it has yet to succeed in video dense prediction. Thus, we focus on tasks such as object tracking and semantic segmentation that require temporally consistent, spatially dense features for each frame. So far, progress in computer vision has been largely driven by static image encoders. Recent efforts have extended self-supervised learning to videos through masked autoencoding [12, 15, 47, 46] and contrastive learning [38, 55]. However, image encoders often outperform video-specific models across various video tasks [1, 34, 41, 52, 39, 49, 50], especially on dense prediction tasks (see Table 1). One explanation is that many video encoders are designed for global representation learning, such as classification, and fail to produce spatially detailed, temporally aligned frame-level features needed for dense prediction. Compounding this issue is the limited diversity and scale of video pretraining datasets compared to their image counterparts. Without such datasets, creating video frame encoders that can effectively capture scene dynamics, remember the past, interpret the present, and anticipate the future remains a significant challenge.

To address this, we propose the FRAME (Feature Representation and Anticipation with MEemory) encoder—a self-supervised video model that combines the strengths of pretrained image encoders with lightweight temporal modeling. Our key insight is that rich visual knowledge from large-scale image models (e.g., DINO, CLIP) can be transferred via feature distillation, avoiding the need for expensive video pretraining from scratch. At the same time, FRAME remains compact and efficient, rather than building on top of heavy image backbones. As shown in Figure 2, FRAME is trained in two stages. In Stage 1, we train a student encoder to match dense patch-level and class-level features from frozen image-based teacher models (DINO and CLIP). In Stage 2, we equip the student with lightweight temporal modules—a memory unit that aggregates past context and an anticipation unit that predicts future features. This two-stage design preserves the spatial fidelity of image representations while introducing temporal consistency needed for dense video tasks.

To our knowledge FRAME is the first student video encoder distilled from image teachers that outperforms both the original image-only models (e.g., DINO, DINOv2) and prior self-supervised video encoders on frame-level dense prediction tasks such as semantic segmentation and label propagation. Additionally, we also align FRAME’s class token with CLIP’s semantic space, enabling compatibility with language-driven objectives with minimal overhead. We validate this with video action classification as an initial baseline. *Our results suggest that distilling image knowledge with lightweight temporal adaptation could be a scalable path for learning high-quality video representations in a self-supervised manner.*

In summary, our main contributions are:

- **Model Architecture:** We propose FRAME, a self-supervised video frame encoder that distills dense spatial and semantic features from pretrained image models (e.g., DINO, DINOv2, CLIP), and extends them into effective video encoders using lightweight memory and anticipation modules. The resulting model(s) produces temporally consistent per-frame representations and offers a practical foundation for dense video prediction tasks.
- **Performance Advancement:** FRAME achieves state-of-the-art performance on dense video tasks—including semantic segmentation, label propagation, and visual correspondence—surpassing both image-only encoders and prior self-supervised video models.
- **Empirical Insights:** We conduct an extensive study of design factors, covering architectural and training choices such as encoder/decoder depth, input resolution, training duration, data size, and stage-wise training strategy. Code, model checkpoints, and training recipes will be released.

2 Related Works

Our approach integrates three key research areas: self-supervised visual representation learning, adaptation of image representations to video domains, and learning visual correspondence in videos.

Self-supervised Learning in Vision. Self-supervised learning (SSL) has emerged as a powerful framework for learning visual representations without labels. Early methods relied on proxy tasks like patch ordering [11] or frame shuffling [31], while more recent work focuses on contrastive learning [18], masked autoencoding [19], and self-distillation [4, 32]. While masked autoencoders (e.g., MAE [19]) excel at global representation learning, they struggle with dense prediction tasks. In contrast, DINO [4, 32] achieves strong spatial correspondence and has become a preferred backbone for tasks like segmentation and tracking. Surprisingly, despite being trained only on images, DINO and similar image-based models often outperform video-specific self-supervised methods on dense prediction tasks (Table 1). Even video adaptations such as VideoMAE [46] fail to close this gap. This

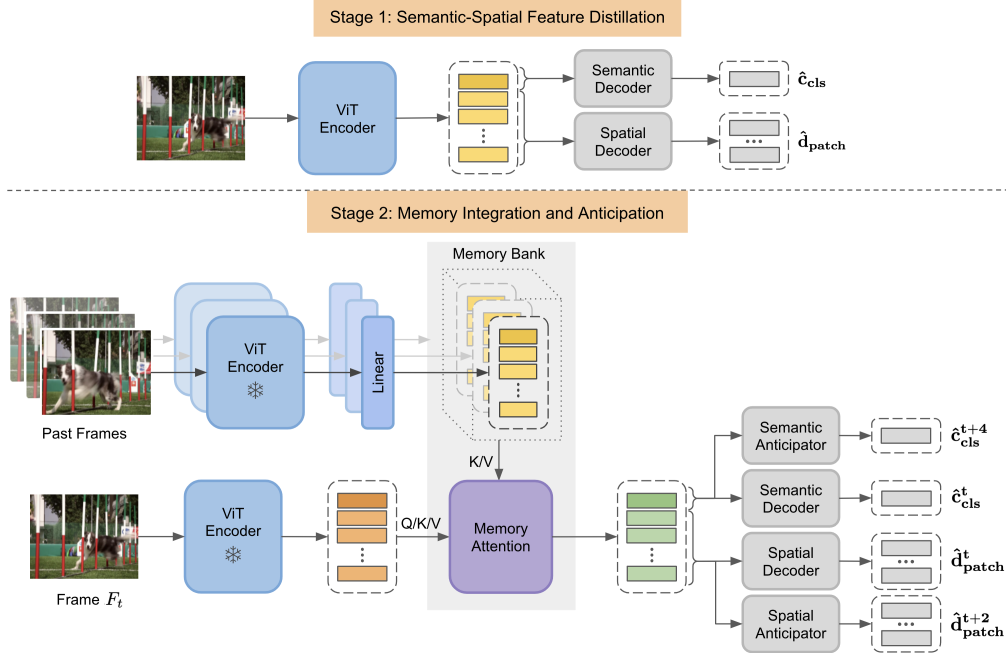


Figure 2: **Overview of FRAME Architecture and Two-Stage Training Process.** In Stage 1, the encoder is trained to jointly distill CLIP features (providing semantic understanding) and DINO features (providing spatial understanding). In Stage 2, this pre-trained encoder processes the past and current frames and the model is optimized for memory integration and future anticipation.

performance gap motivates our approach: rather than relying solely on large-scale video pretraining, we distill spatial and semantic features from pretrained image models, and enhance them with lightweight temporal modules for dense prediction.

Extending Image Representations to Video. Recent work has explored adapting image-based self-supervised methods to video tasks by modeling temporal relationships. SiamMAE [15] and CropMAE [12] extend masked image modeling to videos, but remain limited to pairwise frame relationships and require re-learning representations from scratch. DINO-Tracker [47] instead fine-tunes pre-trained DINO [4] for video correspondence, while contrastive video methods [55, 13, 43] depend on carefully tuned augmentations [54] and collapse-prevention mechanisms [17, 5, 6]. Other works use frozen image encoders and introduce auxiliary modules for temporal modeling [36, 10], but often fail to target video dense prediction. In contrast, FRAME distills spatial features from DINO and semantic features from CLIP into a per-frame encoder without retraining or fine-tuning. While recent work explores similar distillation strategies for images [37, 42], we demonstrate their effectiveness in video. Our method goes beyond pairwise modeling by incorporating memory and anticipation modules, yielding temporally consistent and predictive features critical for dense video prediction.

Visual Correspondence Learning. Visual correspondence spans fine-grained (pixel/part) and object-level tracking, supporting tasks like video object segmentation [33, 57], part propagation, and pose tracking [59, 22]. Traditional methods rely on supervision [2, 48, 9, 8, 23, 53], limiting scalability due to annotation cost. While self-supervised learning has matched supervised performance in static images [4, 32], similar success in videos—especially for dense, spatio-temporal tasks—remains limited. Our approach addresses this by leveraging strong image encoders and introducing memory-based temporal modeling, enabling correspondence learning without labels.

3 FRAME

Our goal is to train a video frame encoder that captures spatial and semantic details from the current frame, enriched with temporal context from the past and anticipatory cues for the future. To this end, we adopt a two-stage training approach (Figure 2): Stage 1 (Section 3.1) distills semantic and spatial features from individual frames, yielding a strong frame encoder; Stage 2 (Section 3.2) infuses

the ability to capture past context and anticipate the near future, enabling it to generate temporally consistent frame-wise features.

3.1 Stage 1: Semantic-Spatial Feature Distillation

We train a ViT-based encoder with two lightweight decoders: one to match CLIP’s [CLS] token and another to match DINO’s patch-level features. This stage produces a per-frame encoder with rich semantic and spatial representations.

ViT Encoder. We take the input image $\mathbf{x} \in \mathbb{R}^{H \times W \times 3}$, into $N = HW/P^2$ non-overlapping patches and project each to a D -dimensional embedding, where D is 384 or 768 depending on the backbone (e.g., DINO-S vs DINO-B/DINOv2). These are concatenated with a learnable [CLS] token and positional embeddings to form the sequence $\mathbf{z}_0 \in \mathbb{R}^{(N+1) \times D}$. A 12-layer ViT encoder processes this sequence, producing a [CLS] token for global image representation $\mathbf{y}_{\text{cls}} \in \mathbb{R}^{1 \times D}$ and contextualized patch tokens for local image features $\mathbf{y}_{\text{patch}} \in \mathbb{R}^{N \times D}$.

Semantic Decoder. The semantic decoder is a single linear layer that maps the ViT Encoder’s [CLS] token representation into CLIP’s feature space. Formally, it projects $\mathbf{y}_{\text{cls}} \in \mathbb{R}^{1 \times D}$ to $\hat{\mathbf{c}}_{\text{cls}} \in \mathbb{R}^{1 \times D^c}$, where D^c denotes CLIP’s feature dimension size.

Spatial Decoder. The spatial decoder is a single block Transformer that operates on the N patch tokens generated by the ViT to project them into DINO’s feature space. Formally, it processes $\mathbf{y}_{\text{patch}} \in \mathbb{R}^{N \times D}$ to produce $\hat{\mathbf{d}}_{\text{patch}} \in \mathbb{R}^{N \times D^d}$, where D^d denotes DINO’s feature dimension size.

Training. The encoder and the decoders are jointly trained in an end-to-end manner using the following loss function:

$$\mathcal{L} = \lambda_1 \left(1 - \frac{\mathbf{c}_{\text{cls}} \cdot \hat{\mathbf{c}}_{\text{cls}}}{\|\mathbf{c}_{\text{cls}}\| \|\hat{\mathbf{c}}_{\text{cls}}\|} \right) + \lambda_2 \frac{\sum_{\text{patch}} \|\mathbf{d}_{\text{patch}} - \hat{\mathbf{d}}_{\text{patch}}\|^2}{N} \quad (1)$$

We use $\lambda_1 = 1.0$ and $\lambda_2 = 1.0$, \mathbf{c}_{cls} and $\mathbf{d}_{\text{patch}}$ refer to CLIP and DINO teacher outputs, respectively. Both the semantic and spatial decoders are intentionally kept lightweight to encourage the encoder to produce directly usable representations, rather than offloading learning to the decoders.

To ensure balanced learning, we normalize both loss components via mean scaling and apply cosine annealing with warm restarts to avoid convergence to local minima. These strategies improve class token alignment with CLIP. We also investigate loss dropout—temporarily disabling one loss component—and gradient-based loss balancing, with details provided in the supplementary material.

Inference. Once training is complete, the decoders are discarded. The encoder is retained as a compact image backbone that produces both semantic and spatially rich features for each frame, which are used for encoding in the next stage.

3.2 Stage 2: Memory Integration and Anticipation

While Stage 1 produces rich features for individual frames, video tasks require representations that are temporally consistent and predictive. Stage 2 addresses this by introducing temporal context through a memory module that integrates past frame information and anticipates near-future representations—critical for dynamic agents where processing delays necessitate short-term forecasting. We freeze the ViT encoder from Stage 1 and use it to extract features from the current and past frames. These are fused via a memory block to produce temporally enriched representations for the current frame. Future frame features serve as a self-supervised signal to guide this integration.

Memory Block. The memory block consists of two components: a memory bank and a memory attention module. The memory bank is a first-in-first-out (FIFO) queue that stores the encoding of the past frames, and the memory attention module is trained to enrich the current frame’s representations with the context derived from past frames. When encoding a frame F_t at timestep t , the memory bank stores encodings of previous $m = 5$ frames using the frozen ViT encoder from Stage 1. Each frame yields a set of patch tokens $\in \mathbb{R}^{N \times D}$, where D is the feature dimension (e.g., 384 for DINO-S, 768 for DINO-B/DINOv2). To focus on essential information, each token is passed through a linear projection to a lower-dimensional space ($d = 64$), forming a compact representation that acts as a bottleneck to retain salient temporal features, particularly inspired by the memory attention block of SAM 2 [40]. These reduced features are stored in a FIFO memory bank, which is continuously

updated as new frames are processed. To encode positional context, we enrich these features with spatio-temporal positional embeddings that encode both patch location and frame timestamp.

Memory Attention Module. To integrate information from memory, we concatenate all stored frame features along the token dimension and apply a linear projection to produce consolidated memory embeddings. These are fed into a cross-attention module alongside the current frame’s features. Here, queries come from the current frame, while keys and values are derived from the memory bank and the current frame itself. This mechanism enables the encoder to dynamically attend to relevant past information when computing the current representation. To further refine the output, we follow the cross-attention with a self-attention block applied over the updated current frame features. The resulting features from this module serve as temporally enriched representations that support downstream tasks requiring frame-to-frame consistency and short-term prediction.

Semantic and Spatial Decoders. To train the memory-augmented encoder to model temporal consistency and short-term anticipation, we use four lightweight decoders: (1) A *semantic decoder* to predict CLIP-like global features $\hat{\mathbf{c}}_{\text{cls}}^t$ for the current frame F_t , (2) a *semantic anticipator* to anticipate CLIP-like global features $\hat{\mathbf{c}}_{\text{cls}}^{t+4}$ for the future frame F_{t+4} , (3) a *spatial decoder* to predict DINO-like patch-level features $\hat{\mathbf{d}}_{\text{patch}}^t$ for the current frame F_t , and (4) a *spatial anticipator* to anticipate DINO-like patch-level features $\hat{\mathbf{d}}_{\text{patch}}^{t+2}$ for the future frame F_{t+2} . These decoders force the current frame representation to encode predictive signals for future frames. The selection of the future frame to anticipate is informed by an experiment measuring the variability of CLIP and DINO features across consecutive video frames (details provided in the supplementary). We choose a frame delta that demonstrates moderate changes – enough for meaningful learning without overwhelming the model. In our analysis, CLIP features exhibit slower variation due to the gradual change of global information, while DINO features fluctuate more rapidly due to their sensitivity to local patch-level changes.

Training. We train the memory attention module, linear projection layers, and decoders using the following loss:

$$\mathcal{L} = \alpha_1 \left(1 - \frac{\mathbf{c}_{\text{cls}}^t \cdot \hat{\mathbf{c}}_{\text{cls}}^t}{\|\mathbf{c}_{\text{cls}}^t\| \|\hat{\mathbf{c}}_{\text{cls}}^t\|} \right) + \alpha_2 \left(1 - \frac{\mathbf{c}_{\text{cls}}^{t+4} \cdot \hat{\mathbf{c}}_{\text{cls}}^{t+4}}{\|\mathbf{c}_{\text{cls}}^{t+4}\| \|\hat{\mathbf{c}}_{\text{cls}}^{t+4}\|} \right) + \alpha_3 \frac{\sum_{\text{patch}} \|\mathbf{d}_{\text{patch}}^t - \hat{\mathbf{d}}_{\text{patch}}^t\|^2}{N} + \alpha_4 \frac{\sum_{\text{patch}} \|\mathbf{d}_{\text{patch}}^{t+2} - \hat{\mathbf{d}}_{\text{patch}}^{t+2}\|^2}{N} \quad (2)$$

Here, $\alpha_1 = 0.2$, $\alpha_2 = 0.1$, $\alpha_3 = 2.0$, $\alpha_4 = 0.4$, and $\mathbf{c}_{\text{cls}}^i$ and $\mathbf{d}_{\text{patch}}^i$ are the CLIP and DINO features of i^{th} frame. These weights ($\alpha_1, \alpha_2, \alpha_3, \alpha_4$) were empirically determined based on results from a subset of DAVIS [33] dataset.

3.3 Task-Specific Feature Adaptation

At inference time, we discard all decoders and use only the patch and [CLS] token outputs from the memory attention module (Figure 2) for downstream tasks 3d. For tasks requiring fine-grained spatial-temporal reasoning—such as label propagation, semantic segmentation, and pose tracking—we use the patch tokens. For tasks requiring global frame-level understanding—such as video action classification—we use the [CLS] token. For zero-shot classification aligned with CLIP (e.g., prompt-based action recognition), we project the [CLS] token into CLIP space using the semantic decoder $\hat{\mathbf{c}}_{\text{cls}}^t$ of the current frame. This dual-mode design enables FRAME to support both zero-shot and trainable downstream tasks without modifying the encoder backbone.

4 Experiments

We evaluate FRAME’s representation on three categories of video tasks: (1) **visual correspondence**—including video object segmentation, semantic part propagation, and pose tracking—to assess the model’s ability to learn fine-grained, temporally consistent correspondences; (2) **semantic segmentation**, to evaluate spatial precision and temporal coherence; and (3) **action classification**, to assess global frame-level action categorization.

Training details. As a self-supervised method, FRAME can be trained on any video data. We primarily train on 80,000 videos from Kinetics-400 [24] (uniformly sampled per class) and 700

Table 1: **Semi-supervised visual correspondence task comparison.** We compare performance on DAVIS [33], VIP [59], and JHMDB [22] datasets where FRAME substantially outperforms.

Method	Backbone	Dataset	Type	DAVIS			VIP	JHMDB
				$J \& F_m$	J_m	F_m	mIoU	PCK@0.1 / PCK@0.2
SimSiam [7]	ResNet-50	ImageNet	Image	66.3	64.5	68.2	35.0	58.4 / 77.5
MoCo [16]	ResNet-50	ImageNet	Image	65.4	63.2	67.6	36.1	60.4 / 79.3
TimeCycle [51]	ResNet-50	VLOG	Video	40.7	41.9	39.4	28.9	57.7 / 78.5
UVC [29]	ResNet-50	Kinetics	Video	56.3	54.5	58.1	34.2	56.0 / 76.6
VFS [55]	ResNet-50	Kinetics	Video	68.9	66.5	71.3	43.2	60.9 / 80.7
MAE [19]	ViT-B/16	ImageNet	Image	53.5	52.1	55.0	28.1	44.6 / 73.4
VideoMAE [46]	ViT-S/16	Kinetics	Video	39.3	39.7	38.9	23.3	41.0 / 67.9
DINO [4]	ViT-S/16	ImageNet	Image	61.8	60.2	63.4	36.2	45.6 / 75.0
SiamMAE [15]	ViT-S/16	Kinetics	Video	62.0	60.3	63.7	37.3	47.0 / 76.1
FRAME	ViT-S/16	Kinetics	Video	65.7	62.1	69.2	41.2	48.7 / 79.2
FRAME	ViT-S/16	Kinetics+Ego4D	Video	66.3	62.9	69.8	42.0	49.0 / 79.3
DINO [4]	ViT-S/8	ImageNet	Image	69.9	66.6	73.1	39.5	56.5 / 80.3
SiamMAE [15]	ViT-S/8	Kinetics	Video	71.4	68.4	74.5	45.9	61.9 / 83.8
FRAME	ViT-S/8	Kinetics	Video	73.2	69.5	77.0	47.9	64.1 / 85.9
FRAME	ViT-S/8	Kinetics+Ego4D	Video	74.4	69.9	79.0	48.2	64.3 / 86.0

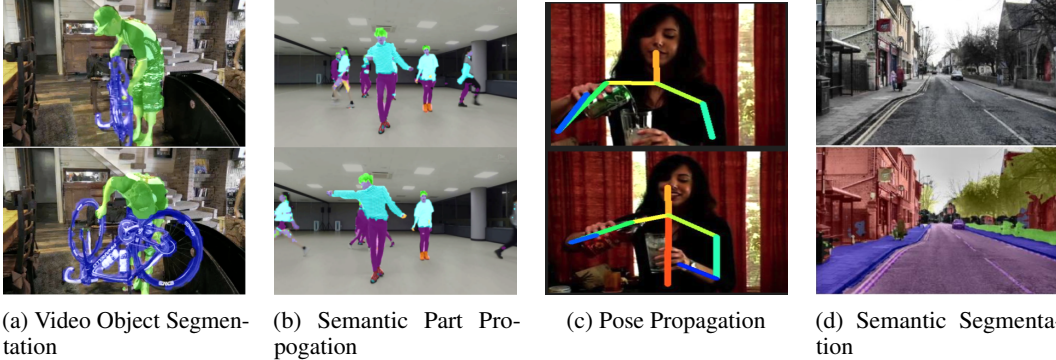


Figure 3: **Examples of correspondence and segmentation tasks** (a) Video object segmentation: initial (top) and propagated (bottom) frames. (b) Semantic part propagation: initial (top) and propagated (bottom) frames. (c) Pose propagation: initial (top) and propagated (bottom) poses. (d) Semantic segmentation: original image (top) and segmentation overlay (bottom).

randomly sampled videos from Ego4D [14]. We repeat training with four different Ego4D subsets to measure variability and also report results using the full Ego4D and Kinetics dataset in the supplementary. We found that performance remained largely stable after a certain threshold of training videos and epochs. All models are trained for 70 epochs using 400×400 resized frames. We report results from two main variants: one trained on Kinetics only, and one trained on Kinetics + Ego4D, with the latter consistently outperforming due to increased data diversity. An extended data ablation—including results with SA-V [40]—is provided in the supplementary.

Visual Correspondence Tasks. To assess the FRAME encoder’s feature quality, we use three semi-supervised video propagation tasks: object segmentation on DAVIS-2017 [33], semantic part tracking on VIP [59], and pose tracking on JHMDB [22]. Starting with a ground truth mask for the first frame, we propagate it through the video using patchwise k-nearest neighbor matching from each frame to the next. We use this simple propagation technique to isolate the effectiveness of FRAME to produce temporally consistent features and to enable direct comparison with previous pretrained encoders. This evaluation is not intended to showcase the best possible performance via task-specific tuning. Instead, it aims to assess feature quality under a standard setting consistent with the literature [20, 15, 55, 12]. Our results for these tasks are in Table 1, with results for some comparison methods

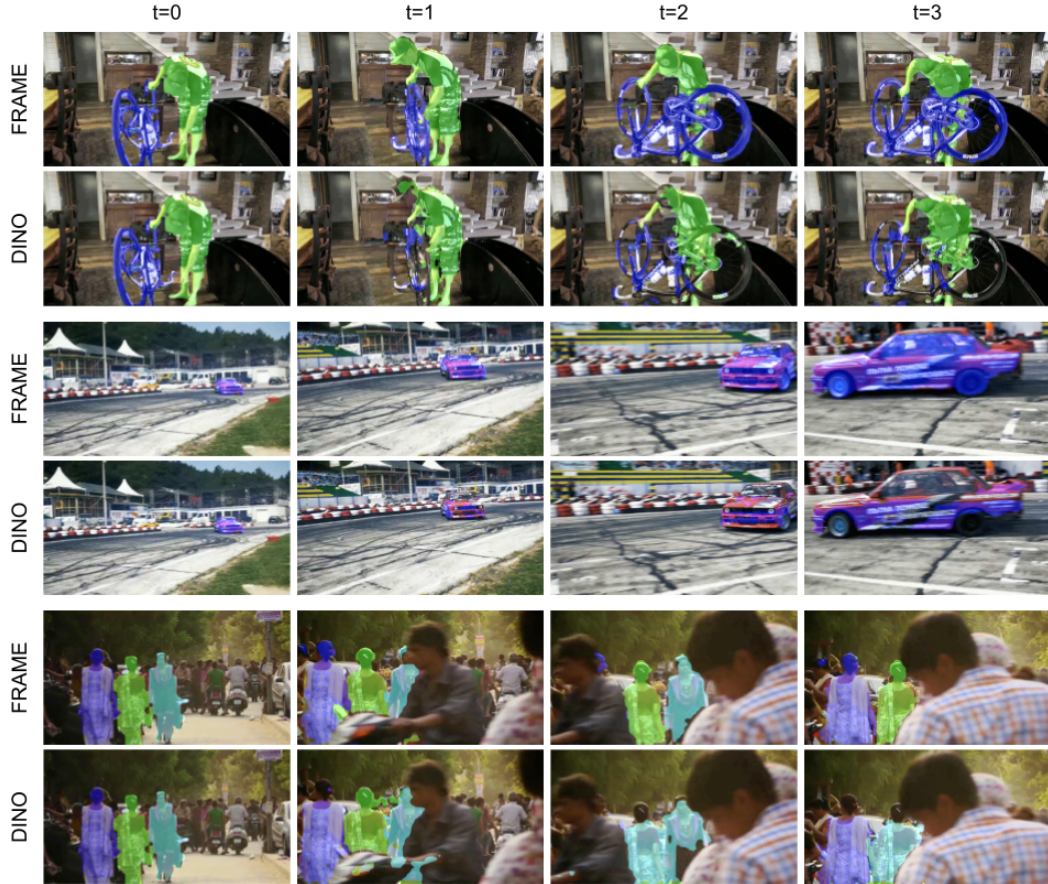


Figure 4: **Comparison of FRAME and DINO on feature propagation across video frames.** FRAME demonstrates greater robustness to viewpoint changes, occlusions, and object reappearances, making it a more suitable video frame encoder.

drawn from a similar table in [15]. In the supplemental, we provide videos comparing FRAME and DINO, along with an extended label propagation table that highlights: (1) performance gains from ViT-S to ViT-B across tasks, (2) gains over DINOv1 and DINOv2 across different patch sizes, and (3) runtime, parameter count, and memory usage details.

Video Object Segmentation. We evaluate FRAME on the DAVIS-2017 [33] benchmark for semi-supervised multi-object video segmentation. Consistent with previous methods [15, 21, 12], we use 480p images and the standard evaluation setup for comparability. Performance is measured by the Jaccard Index, which assesses the overlap between the predicted and ground truth masks, and the boundary accuracy, which evaluates how closely the predicted

mask aligns with the object’s boundaries. FRAME outperforms SiamMAE [15], 65.7 vs. 62.0 with a patch size of 16, and 73.2 vs. 71.4 with a patch size of 8, indicating strong feature quality and consistency in segmentation (Table 1). While task-specific fine-tuned models still outperform[9], FRAME significantly narrows the gap to these specialized methods—despite using simple label propagation and no task-specific tuning or learned memory modules for inference. As an auxiliary experiment to demonstrate that FRAME can approach models trained on large-scale video segmentation data, we pool region tokens from FRAME features using class-agnostic SAM[26] masks and track objects via cosine similarity to the first-frame token, following the region-based representation paradigm [44]. Results in Table 3 show that FRAME outperforms DINO variants and approaches SAM 2. These

Table 2: **Video activity classification comparison.** FRAME performs comparably to CLIP in both zero-shot and linear classification.

Model	Zero-Shot (%)		Linear (%)	
	HMDB-51	UCF-101	HMDB-51	UCF-101
CLIP	52.7	59.1	76.2	69.5
FRAME S/16	52.1	58.5	76.1	69.7
FRAME B/16	52.4	58.9	77.5	69.3

Table 3: **Performance on DAVIS ($J \& F_m$).** FRAME uses region-based representations [44] to track objects from a single annotated frame, outperforming DINO variants and approaching task-specific models like SAM 2.(details in appendix)

Model	DAVIS ($J \& F_m$)
SAM 2	90.7
DINO ViT-S/8	80.7
FRAME ViT-S/8	84.4
DINO ViT-B/8	85.6
FRAME ViT-B/8	88.1

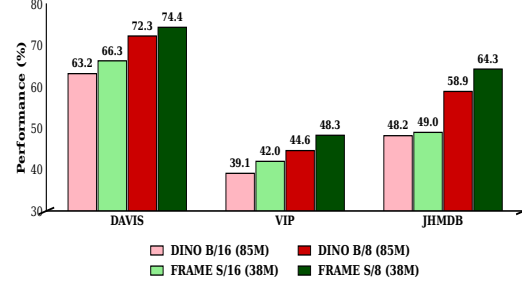


Figure 5: **Comparison of FRAME and DINO across model scales.** FRAME outperforms DINO with fewer parameters.

results suggest that FRAME + SAM 2 could enable a more memory-efficient many-object tracking. See supplementary for additional details of the experiment.

Semantic Part Propagation. Next, we evaluate FRAME on the Video Instance Parsing (VIP) [59] benchmark, a task that involves propagating semantic masks for 20 different human parts. The VIP dataset presents unique challenges compared to others in our evaluation due to its much longer video durations (up to 120 seconds). Following the protocol from prior work [28], we use images at 560×560 resolution and rely on a single context frame for evaluation. On this challenging dataset, our ViT-S/16 model and ViT-S/8 variants outperform prior methods, with a mean Intersection-over-Union (mIoU) improvement over prior self-supervised SotA SiamMAE [15], from 37.3 to 41.2 and 45.9 to 47.9 respectively (Table 1). The mIoU metric measures the overlap between predicted and ground truth masks, capturing the model’s accuracy in segmenting and tracking each human part.

Human Part Propagation. We evaluate FRAME on the keypoint propagation task, which requires the accurate spatial tracking of 15 keypoints across frames. This task demands highly precise correspondence between frames to correctly propagate keypoint locations. Following the protocol from prior work [28], we use 320×320 images and a single context frame for evaluation. FRAME surpasses all previous methods in this task, with FRAME (S/16) improving PCK@0.1 by 1.7% and FRAME (S/8) by 2.4% over SiamMAE [15] (Table 1). PCK@0.1 assesses keypoint accuracy within 10% of the object’s bounding box, while PCK@0.2 allows a 20% margin. Higher PCK scores indicate better spatial correspondence and keypoint tracking precision.

Video Semantic Segmentation. We evaluate video semantic segmentation on CamVid [3] and VSPW [30], covering urban and diverse real-world scenes. A linear decoder is trained atop DINO [4], DINOv2 [32], and FRAME features. As shown in Table 4, FRAME outperforms all prior self-supervised encoders across backbones. With ViT-S/8, FRAME improves over DINO by 3.0% (current) and 2.9% (future) on CamVid, and by 2.8% and 1.6% on VSPW. With ViT-L/14, it surpasses DINOv2 by 1.5–3.5% across tasks. When paired with a U-Net decoder (Table 18 (supplemental)), FRAME achieves 79.1 mIoU on CamVid and 52.3 on VSPW—trailing task-specific state-of-the-art methods, but that is not our primary goal. Rather, our goal is to demonstrate that FRAME provides a general-purpose dense representation that can approach or match SotA when paired with strong decoders, for eg. improving over DINOv2 by up to 4.8%. Figure 6 extends this analysis to future-frame prediction on CamVid. FRAME consistently outperforms DINO, with a growing advantage at $t + 3$, surpassing its $t + 2$ training objective. This highlights FRAME’s ability to capture temporal structures, enhancing predictive robustness.

Video Action Classification. To assess suitability for video action classification, we evaluate on HMDB-51 [27] and UCF-101 [45] (Table 2). For zero-shot evaluation, we sample eight frames, extract CLS tokens from either CLIP ViT-B/32 [35] or the FRAME (S/16) semantic decoder, and average them into a 1×512 video representation. Cosine similarity with text-encoded action labels (e.g., “a person *brushing*”) is used for prediction. FRAME achieves performance comparable to CLIP, despite being trained only on Kinetics-400 [24]. In the supervised setting, a linear classifier on the [CLS] token yields similar results, confirming FRAME’s versatility for classification, segmentation, and correspondence. Additional experiments distilling CLIP ViT-L/14 into FRAME (S/16) and other variants using DINO and DINOv2 backbones are included in the supplementary.

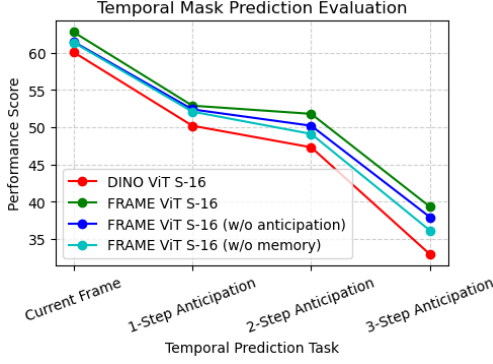


Figure 6: (a) **Semantic segmentation on current and future frames.** FRAME outperforms DINO on CamVid. Removing memory or anticipation reduces performance, showing their complementary role in temporal reasoning.

Table 4: (b) **Video semantic segmentation results on CamVid and VSPW.** FRAME outperforms other self-supervised methods on both datasets and tasks.

Model	CamVid (mIoU)		VSPW (mIoU)	
	Curr.	Future	Curr.	Future
DINO ViT-S/16	60.1	50.2	36.4	25.6
SiamMAE ViT-S/16	59.5	47.8	34.7	24.9
CatMAE ViT-S/16	58.9	46.2	35.1	25.1
CropMAE ViT-S/16	56.4	47.9	35.8	23.7
FRAME ViT-S/16	62.8	53.9	38.9	28.3
DINO ViT-S/8	59.6	51.1	35.9	25.8
CatMAE ViT-S/8	58.9	50.5	34.7	25.4
FRAME ViT-S/8	62.6	54.0	38.0	27.4
DINOv2 ViT-L/14	68.3	56.1	41.8	30.3
FRAME ViT-L/14	69.8	59.2	44.0	33.8

Ablations. In Table 5, we analyze the impact of key components of the FRAME encoder: the stagewise training, use of memory, anticipation loss, and training data. Memory and anticipation substantially boost the visual correspondence tasks. They do not help video clip action classification (HMDB, UCF) because all frames are available at once for that task. Re-using and freezing the Stage 1 ViT Encoder for Stage 2 provides the best results, considering the added efficiency in training and that using the same ViT encoder for past and current frame encoding saves computation and memory. The inclusion of Ego4d videos in pretraining further boosts performance by adding diversity, with tasks like semantic segmentation on CamVid benefiting the most.

Table 5: **Ablations.** Our method (blue highlight) is two-stage training, where Stage 1 trains the per-frame ViT Encoder, and then Stage 2 trains the Memory Attention module to anticipate using memory. We compare to using only the Stage 1 ViT Encoder (“Stage 1”), training the stage 2 ViT random with initialization (“Stage 2 Scratch”), fine-tuning the ViT in the second stage (“2-Stage FT”), or re-using the frozen Stage 1 ViT in Stage 2 (“2-Stage”). We choose the last for efficiency and good results. Adding more data (+Ego4D) helps, and memory and learning to anticipate help for dense prediction tasks.

Memory	Anticipation	Stages	Data	DAVIS	VIP	JHMDB	CamVid	HMDB	UCF
				<i>J&F</i>	mIoU	PCK	mIoU	Acc.	Acc.
		Stage 1	Kinetics	62.1	39.0	46.6	59.9	52.9	56.9
✓	✓	Stage 2 Scratch	Kinetics	65.4	40.4	62.3	61.9	50.9	56.2
✓	✓	2-Stage FT	Kinetics	65.7	41.6	48.5	61.5	51.1	59.7
✓	✓	2-Stage	Kinetics	65.7	41.2	48.7	61.6	49.7	56.3
		2-Stage	Kin.+Ego4D	62.6	39.2	46.7	60.1	-	-
✓		2-Stage	Kin.+Ego4D	65.5	41.2	48.6	62.3	51.4	59.3
✓	✓	2-Stage	Kin.+Ego4D	66.3	42.0	49.0	62.8	52.1	58.9

See the Supplemental for many more ablations, including: number of memory frames, dataset size, encoder depth, decoder depth, number of training epochs, and training image resolution.

5 Conclusion

We introduce FRAME, a self-supervised video frame encoder that distills dense spatial and semantic features into more compact backbones and enhances them with lightweight memory and anticipation modules. FRAME delivers state-of-the-art performance on a range of dense video prediction tasks while maintaining a compact and efficient architecture. By aligning both patch-level and semantic representations, it offers a practical foundation for temporally consistent video understanding.

Limitations. We show FRAME’s features are strong in a frozen setting but do not evaluate their performance under fine-tuning, though this is consistent with prior self-supervised work like DINO.

Future work. Includes integrating FRAME into video-language models as a drop-in backbone and extending its memory design to better encode fine-grained motion and long-term dynamics for complex video understanding.

6 Acknowledgment

This work is supported in part by awards ONR N00014-23-1-2383 and DARPA HR0011-23-9-0060. The views and conclusions expressed are those of the authors, and not necessarily representative of the US Government or its agencies.

References

- [1] G. Aydemir, W. Xie, and F. Güney. Self-supervised object-centric learning for videos. *ArXiv*, abs/2310.06907, 2023. URL <https://api.semanticscholar.org/CorpusID:263835208>.
- [2] L. Bertinetto, J. Valmadre, J. F. Henriques, A. Vedaldi, and P. H. S. Torr. Fully-convolutional siamese networks for object tracking, 2021. URL <https://arxiv.org/abs/1606.09549>.
- [3] G. J. Brostow, J. Shotton, J. Fauqueur, and R. Cipolla. Segmentation and recognition using structure from motion point clouds. In *ECCV (I)*, pages 44–57, 2008.
- [4] M. Caron, H. Touvron, I. Misra, H. Jégou, J. Mairal, P. Bojanowski, and A. Joulin. Emerging properties in self-supervised vision transformers, 2021. URL <https://arxiv.org/abs/2104.14294>.
- [5] T. Chen, S. Kornblith, M. Norouzi, and G. Hinton. A simple framework for contrastive learning of visual representations, 2020. URL <https://arxiv.org/abs/2002.05709>.
- [6] X. Chen and K. He. Exploring simple siamese representation learning, 2020. URL <https://arxiv.org/abs/2011.10566>.
- [7] X. Chen and K. He. Exploring simple siamese representation learning. *arXiv preprint arXiv:2011.10566*, 2020.
- [8] H. K. Cheng, S. W. Oh, B. Price, A. Schwing, and J.-Y. Lee. Tracking anything with decoupled video segmentation, 2023. URL <https://arxiv.org/abs/2309.03903>.
- [9] H. K. Cheng, S. W. Oh, B. Price, J.-Y. Lee, and A. Schwing. Putting the object back into video object segmentation, 2024. URL <https://arxiv.org/abs/2310.12982>.
- [10] I. R. Dave, S. Jenni, and M. Shah. No more shortcuts: Realizing the potential of temporal self-supervision. In *Proceedings of the AAAI Conference on Artificial Intelligence*, volume 38, pages 1481–1491, 2024.
- [11] C. Doersch, A. Gupta, and A. A. Efros. Unsupervised visual representation learning by context prediction. In *Proceedings of the IEEE international conference on computer vision*, pages 1422–1430, 2015.
- [12] A. Eymaël, R. Vandeghen, A. Cioppa, S. Giancola, B. Ghanem, and M. V. Droogenbroeck. Efficient image pre-training with siamese cropped masked autoencoders, 2024. URL <https://arxiv.org/abs/2403.17823>.
- [13] C. Feichtenhofer, H. Fan, B. Xiong, R. Girshick, and K. He. A large-scale study on unsupervised spatiotemporal representation learning, 2021. URL <https://arxiv.org/abs/2104.14558>.
- [14] K. Grauman, A. Westbury, E. Byrne, Z. Chavis, A. Furnari, R. Girdhar, J. Hamburger, H. Jiang, M. Liu, X. Liu, M. Martin, T. Nagarajan, I. Radosavovic, S. K. Ramakrishnan, F. Ryan, J. Sharma, M. Wray, M. Xu, E. Z. Xu, C. Zhao, S. Bansal, D. Batra, V. Cartillier, S. Crane, T. Do, M. Doulaty, A. Erapalli, C. Feichtenhofer, A. Fragomeni, Q. Fu, C. Fuegen, A. K. Gebreselasie, C. González, J. M. Hillis, X. Huang, Y. Huang, W. Jia, W. Khoo, J. Kolár, S. Kottur, A. Kumar, F. Landini, C. Li, Y. Li, Z. Li, K. Mangalam, R. Modhugu, J. Munro, T. Murrell, T. Nishiyasu, W. Price, P. R. Puentes, M. Ramazanov, L. Sari, K. K. Somasundaram, A. Southerland, Y. Sugano, R. Tao, M. Vo, Y. Wang, X. Wu, T. Yagi, Y. Zhu, P. Arbeláez, D. J. Crandall, D. Damen, G. M. Farinella, B. Ghanem, V. K. Ithapu, C. V. Jawahar, H. Joo, K. Kitani, H. Li, R. A. Newcombe, A. Oliva, H. S. Park, J. M. Rehg, Y. Sato, J. Shi, M. Z. Shou, A. Torralba, L. Torresani, M. Yan, and J. Malik. Ego4d: Around the world in 3,000 hours of egocentric video. *CVPR*, 2021.
- [15] A. Gupta, J. Wu, J. Deng, and L. Fei-Fei. Siamese masked autoencoders. In *NeurIPS*, 2023.
- [16] K. He, H. Fan, Y. Wu, S. Xie, and R. Girshick. Momentum contrast for unsupervised visual representation learning. *arXiv preprint arXiv:1911.05722*, 2019.
- [17] K. He, H. Fan, Y. Wu, S. Xie, and R. Girshick. Momentum contrast for unsupervised visual representation learning, 2020. URL <https://arxiv.org/abs/1911.05722>.

- [18] K. He, H. Fan, Y. Wu, S. Xie, and R. Girshick. Momentum contrast for unsupervised visual representation learning. In *Proceedings of the IEEE/CVF conference on computer vision and pattern recognition*, pages 9729–9738, 2020.
- [19] K. He, X. Chen, S. Xie, Y. Li, P. Dollár, and R. Girshick. Masked autoencoders are scalable vision learners, 2021. URL <https://arxiv.org/abs/2111.06377>.
- [20] A. Jabri, A. Owens, and A. A. Efros. Space-time correspondence as a contrastive random walk, 2020. URL <https://arxiv.org/abs/2006.14613>.
- [21] A. Jabri, A. Owens, and A. A. Efros. Space-time correspondence as a contrastive random walk, 2020. URL <https://arxiv.org/abs/2006.14613>.
- [22] H. Jhuang, J. Gall, S. Zuffi, C. Schmid, and M. J. Black. Towards understanding action recognition. In *2013 IEEE International Conference on Computer Vision*, pages 3192–3199, 2013. doi: 10.1109/ICCV.2013.396.
- [23] N. Karaev, I. Rocco, B. Graham, N. Neverova, A. Vedaldi, and C. Rupprecht. Cotracker: It is better to track together, 2024. URL <https://arxiv.org/abs/2307.07635>.
- [24] W. Kay, J. Carreira, K. Simonyan, B. Zhang, C. Hillier, S. Vijayanarasimhan, F. Viola, T. Green, T. Back, P. Natsev, M. Suleyman, and A. Zisserman. The kinetics human action video dataset, 2017. URL <https://arxiv.org/abs/1705.06950>.
- [25] S. Khosla, S. T. V. A. Schwing, and D. Hoiem. Relocate: A simple training-free baseline for visual query localization using region-based representations, 2024. URL <https://arxiv.org/abs/2412.01826>.
- [26] A. Kirillov, E. Mintun, N. Ravi, H. Mao, C. Rolland, L. Gustafson, T. Xiao, S. Whitehead, A. C. Berg, W.-Y. Lo, P. Dollár, and R. Girshick. Segment anything, 2023. URL <https://arxiv.org/abs/2304.02643>.
- [27] H. Kuehne, H. Jhuang, E. Garrote, T. Poggio, and T. Serre. Hmdb: A large video database for human motion recognition. In *2011 International Conference on Computer Vision*, pages 2556–2563, 2011. doi: 10.1109/ICCV.2011.6126543.
- [28] X. Li, S. Liu, S. D. Mello, X. Wang, J. Kautz, and M.-H. Yang. Joint-task self-supervised learning for temporal correspondence, 2019. URL <https://arxiv.org/abs/1909.11895>.
- [29] X. Li, S. Liu, S. D. Mello, X. Wang, J. Kautz, and M.-H. Yang. Joint-task self-supervised learning for temporal correspondence. In *NeurIPS*, 2019.
- [30] J. Miao, Y. Wei, Y. Wu, C. Liang, G. Li, and Y. Yang. Vspw: A large-scale dataset for video scene parsing in the wild. In *2021 IEEE/CVF Conference on Computer Vision and Pattern Recognition (CVPR)*, pages 4131–4141, 2021. doi: 10.1109/CVPR46437.2021.00412.
- [31] I. Misra, C. L. Zitnick, and M. Hebert. Shuffle and learn: unsupervised learning using temporal order verification. In *Computer Vision—ECCV 2016: 14th European Conference, Amsterdam, The Netherlands, October 11–14, 2016, Proceedings, Part I 14*, pages 527–544. Springer, 2016.
- [32] M. Oquab, T. Darcet, T. Moutakanni, H. Vo, M. Szafraniec, V. Khalidov, P. Fernandez, D. Haziza, F. Massa, A. El-Nouby, M. Assran, N. Ballas, W. Galuba, R. Howes, P.-Y. Huang, S.-W. Li, I. Misra, M. Rabbat, V. Sharma, G. Synnaeve, H. Xu, H. Jegou, J. Mairal, P. Labatut, A. Joulin, and P. Bojanowski. DINOv2: Learning robust visual features without supervision, 2024. URL <https://arxiv.org/abs/2304.07193>.
- [33] J. Pont-Tuset, F. Perazzi, S. Caelles, P. Arbeláez, A. Sorkine-Hornung, and L. V. Gool. The 2017 davis challenge on video object segmentation, 2018. URL <https://arxiv.org/abs/1704.00675>.
- [34] R. Qian, S. Ding, X. Liu, and D. Lin. Semantics meets temporal correspondence: Self-supervised object-centric learning in videos. *2023 IEEE/CVF International Conference on Computer Vision (ICCV)*, pages 16629–16641, 2023. URL <https://api.semanticscholar.org/CorpusID:261049053>.
- [35] A. Radford, J. W. Kim, C. Hallacy, A. Ramesh, G. Goh, S. Agarwal, G. Sastry, A. Askell, P. Mishkin, J. Clark, G. Krueger, and I. Sutskever. Learning transferable visual models from natural language supervision, 2021. URL <https://arxiv.org/abs/2103.00020>.
- [36] K. Ranasinghe, M. Naseer, S. Khan, F. S. Khan, and M. S. Ryoo. Self-supervised video transformer. In *Proceedings of the IEEE/CVF Conference on Computer Vision and Pattern Recognition*, pages 2874–2884, 2022.
- [37] M. Ranzinger, G. Heinrich, J. Kautz, and P. Molchanov. Am-radio: Agglomerative vision foundation model reduce all domains into one. In *Proceedings of the IEEE/CVF Conference on Computer Vision and Pattern Recognition*, pages 12490–12500, 2024.
- [38] H. Rasheed, M. U. Khattak, M. Maaz, S. Khan, and F. S. Khan. Fine-tuned clip models are efficient video learners, 2023. URL <https://arxiv.org/abs/2212.03640>.
- [39] H. A. Rasheed, M. U. Khattak, M. Maaz, S. H. Khan, and F. S. Khan. Fine-tuned clip models are efficient video learners. *2023 IEEE/CVF Conference on Computer Vision and Pattern Recognition (CVPR)*, pages 6545–6554, 2022. URL <https://api.semanticscholar.org/CorpusID:254366626>.

- [40] N. Ravi, V. Gabeur, Y.-T. Hu, R. Hu, C. Ryali, T. Ma, H. Khedr, R. Rädle, C. Rolland, L. Gustafson, E. Mintun, J. Pan, K. V. Alwala, N. Carion, C.-Y. Wu, R. Girshick, P. Dollár, and C. Feichtenhofer. Sam 2: Segment anything in images and videos, 2024. URL <https://arxiv.org/abs/2408.00714>.
- [41] M. Salehi, E. Gavves, C. G. M. Snoek, and Y. M. Asano. Time does tell: Self-supervised time-tuning of dense image representations. *2023 IEEE/CVF International Conference on Computer Vision (ICCV)*, pages 16490–16501, 2023. URL <https://api.semanticscholar.org/CorpusID:261076544>.
- [42] S. Sameni, K. Kafle, H. Tan, and S. Jenni. Building vision-language models on solid foundations with masked distillation. In *Proceedings of the IEEE/CVF Conference on Computer Vision and Pattern Recognition*, pages 14216–14226, 2024.
- [43] P. Sermanet, C. Lynch, Y. Chebotar, J. Hsu, E. Jang, S. Schaal, and S. Levine. Time-contrastive networks: Self-supervised learning from video, 2018. URL <https://arxiv.org/abs/1704.06888>.
- [44] M. Shlapentokh-Rothman, A. Blume, Y. Xiao, Y. Wu, S. T. V. H. Tao, J. Y. Lee, W. Torres, Y.-X. Wang, and D. Hoiem. Region-based representations revisited, 2024. URL <https://arxiv.org/abs/2402.02352>.
- [45] K. Soomro, A. R. Zamir, and M. Shah. Ucf101: A dataset of 101 human actions classes from videos in the wild, 2012. URL <https://arxiv.org/abs/1212.0402>.
- [46] Z. Tong, Y. Song, J. Wang, and L. Wang. Videomae: Masked autoencoders are data-efficient learners for self-supervised video pre-training, 2022. URL <https://arxiv.org/abs/2203.12602>.
- [47] N. Tumanyan, A. Singer, S. Bagon, and T. Dekel. Dino-tracker: Taming dino for self-supervised point tracking in a single video, 2024. URL <https://arxiv.org/abs/2403.14548>.
- [48] J. Valmadre, L. Bertinetto, J. Henriques, A. Vedaldi, and P. H. S. Torr. End-to-end representation learning for correlation filter based tracking. In *2017 IEEE Conference on Computer Vision and Pattern Recognition (CVPR)*, pages 5000–5008, 2017. doi: 10.1109/CVPR.2017.531.
- [49] M. Wang, J. Xing, and Y. Liu. Actionclip: A new paradigm for video action recognition. *ArXiv*, abs/2109.08472, 2021. URL <https://api.semanticscholar.org/CorpusID:237563206>.
- [50] Q. Wang, J. Du, K. Yan, and S. Ding. Seeing in flowing: Adapting clip for action recognition with motion prompts learning. *Proceedings of the 31st ACM International Conference on Multimedia*, 2023. URL <https://api.semanticscholar.org/CorpusID:260735882>.
- [51] X. Wang, A. Jabri, and A. A. Efros. Learning correspondence from the cycle-consistency of time. In *CVPR*, 2019.
- [52] Y. Wang, X. Shen, Y. Yuan, Y. Du, M. Li, S. X. Hu, J. L. Crowley, and D. Vaufreydaz. Tokencut: Segmenting objects in images and videos with self-supervised transformer and normalized cut. *IEEE Transactions on Pattern Analysis and Machine Intelligence*, 45:15790–15801, 2022. URL <https://api.semanticscholar.org/CorpusID:251979706>.
- [53] Y. Weng, M. Han, H. He, M. Li, L. Yao, X. Chang, and B. Zhuang. Mask propagation for efficient video semantic segmentation, 2023. URL <https://arxiv.org/abs/2310.18954>.
- [54] T. Xiao, X. Wang, A. A. Efros, and T. Darrell. What should not be contrastive in contrastive learning, 2021. URL <https://arxiv.org/abs/2008.05659>.
- [55] J. Xu and X. Wang. Rethinking self-supervised correspondence learning: A video frame-level similarity perspective, 2021. URL <https://arxiv.org/abs/2103.17263>.
- [56] J. Xu, Z. Xiong, and S. P. Bhattacharyya. Pidnet: A real-time semantic segmentation network inspired by pid controllers, 2023. URL <https://arxiv.org/abs/2206.02066>.
- [57] N. Xu, L. Yang, Y. Fan, D. Yue, Y. Liang, J. Yang, and T. Huang. Youtube-vos: A large-scale video object segmentation benchmark, 2018. URL <https://arxiv.org/abs/1809.03327>.
- [58] T. Zhang, X. Tian, Y. Zhou, S. Ji, X. Wang, X. Tao, Y. Zhang, P. Wan, Z. Wang, and Y. Wu. Dvis++: Improved decoupled framework for universal video segmentation, 2023. URL <https://arxiv.org/abs/2312.13305>.
- [59] Q. Zhou, X. Liang, K. Gong, and L. Lin. Adaptive temporal encoding network for video instance-level human parsing, 2018. URL <https://arxiv.org/abs/1808.00661>.

A Supplementary

This section is structured as follows. In appendix B, we analyze the sensitivity of FRAME to various hyperparameters. Specifically, we evaluate the impact of encoder depth (appendix B.1), number of training epochs (appendix B.2), dataset size (appendix B.3), decoder depth (appendix B.4), number of frames used for memory (appendix B.5), and encoder vs. decoder features in pre-training (appendix B.6) on performance. In appendix C, we outline the training methodology employed for FRAME, including hardware setup, optimization strategy, and loss functions. Furthermore, we present our pooled region-based tracking pipeline, discuss its extension to multi-object tracking, and show qualitative examples. Finally, we describe our empirical procedure for selecting the semantic and spatial anticipation frame deltas used during training. The blue highlight in all tables indicates the selected configuration reported in the main paper.

B Hyperparameter Analysis

B.1 Impact of Encoder Depth

Table 6 shows the effect of varying encoder depth on the performance of FRAME. For DAVIS [33], VIP [59], JHMDB [22], and CamVid Brostow et al. [3], we observe a performance increase as the encoder depth increases from 8 to 18 layers. Notably, encoder depths of 10 and 12 both deliver strong results, with 12 being the one reported in the paper (highlighted in bold letters) due to its balance between computational efficiency and performance. While further increases in depth beyond 12 (e.g., to 14 or 18) lead to marginal gains, the increase in computational cost outweighs the slight improvement. However, for HMDB-51 [27] and UCF-101 [45], the trend is less clear, with results fluctuating across different depths.

B.2 Impact of Number of Epochs

Table 7 highlights the sensitivity of FRAME to the number of training epochs. For DAVIS, VIP, JHMDB, and CamVid, there is a increase in performance as the number of epochs increases, peaking at 70 epochs. Beyond this point, performance trends vary, likely due to overfitting. For HMDB-51 and UCF-101, the trend remains unclear. This could be explained by the fact that these datasets use a semantic decoder for the current frame (refer to the Methods section of the main paper), which mimics CLIP features. As a result, they converge very quickly within a few epochs, leading to the observed fluctuations in trends.

B.3 Impact of Dataset Size

Table 8 examines the effect of pretraining dataset size (percentage of Kinetics-400) on downstream task performance. For most datasets, increasing the dataset size up to 40% results in a steady improvement in performance, with DAVIS and VIP particularly benefiting. However, beyond 60%, the trends vary across tasks; while HMDB-51 and UCF-101 show minor gains, the other datasets exhibit less clear or negligible improvements. This suggests that although increasing the dataset size typically improves model performance, the gains diminish beyond a certain threshold, highlighting the potential need for factors like data diversity to further enhance performance.

B.4 Impact of Decoder Depth

Table 15 evaluates the influence of decoder depth on performance. For DAVIS, VIP, JHMDB, and CamVid, a smaller decoder (fewer layers) generally achieves better results. Specifically, a decoder with depth 1 or 2 performs best, as increasing decoder depth leads to a noticeable decline in performance. This suggests that a shallow decoder is important for extracting meaningful features from the encoder. Here, the results correspond to DINO-ViT-S/8.

B.5 Impact of Number of Frames

Table 10 examines the effect of varying the number of past frames used for memory on downstream task performance. Generally, increasing the number of frames up to 4-5 results in improved performance across all datasets, with DAVIS [33], VIP [59], and JHMDB [22] showing the most

significant gains. However, beyond this threshold, performance begins to decline. This suggests that short-term memory is more beneficial for tasks like video object segmentation and video semantic segmentation, where the relationship between past frames and the current frame remains meaningful only within a limited temporal window. After a certain point, the scene or object appearance can change drastically—an object in frame 1 might differ significantly from the same object in frame 8 but could still be similar to frames 4 or 5. This highlights the importance of selecting an optimal temporal context that balances useful continuity while avoiding outdated or irrelevant information.

B.6 Impact of Encoder vs. Decoder Features in Pre-training

Table 11 examines the effect of different pre-training datasets on downstream task performance while comparing features extracted from the encoder and decoder. Across all datasets, the encoder features consistently outperform the decoder features, irrespective of the pre-training dataset. This suggests that the encoder captures richer temporal representations that benefit video object segmentation and video semantic segmentation tasks. The advantage likely stems from the encoder’s ability to model anticipation and memory. Furthermore, adding datasets such as Ego4D and SA-V leads to marginal improvements, particularly in DAVIS, VIP, and JHMDB, indicating that additional pre-training data enhances feature generalization.

C Training Details

Training Setup. We train FRAME using a combination of raw video frames and precomputed features from DINO and CLIP. The model is optimized to predict DINO patch features and CLIP class tokens for the current frame in a sliding window of 7 RGB frames (5 past, 1 current, 1 future). DINO patch features are supervised with a mean squared error (MSE) loss, while CLIP class tokens are trained using cosine embedding loss, applied after feature normalization. Training is conducted on 8–16 NVIDIA A100 GPUs using PyTorch with the *Accelerate* library¹ for multi-GPU distributed data parallelism (DDP), gradient accumulation, and mixed precision (fp16) training via PyTorch AMP. This setup enables efficient large-batch training within memory constraints while improving computational throughput.

We use the Adam optimizer with a learning rate of $1e-4$ and weight decay of $1e-4$, following a cosine annealing schedule with linear warm-up to ensure stable convergence. The training batch size is 8 per GPU, and training runs for up to 70 epochs with early stopping after 5 epochs of no improvement in validation loss. Each training sample is paired with precomputed DINO [4, 32] and CLIP [35] features. We train on two large-scale video datasets: Kinetics [24] and Ego4D [14], using 80% of the data for training and 20% for validation. Data loading is parallelized with 16 workers and pin-memory enabled. All training metrics, including loss breakdowns and validation performance, are logged with wandb. The training pipeline is designed to scale efficiently across large distributed clusters, with built-in support for mixed precision and dynamic learning rate adjustment.

Encoder Depth	DAVIS	VIP	JHMDB	HMDB-51	UCF-101
	$J \& F_m$	mIoU	PCK@0.1	%	%
8	63.5	41.7	47.3	53.3	58.9
10	64.9	41.8	48.6	53.1	59.4
12	66.3	42.0	49.0	52.1	58.5
14	66.7	42.1	49.0	51.3	59.2
18	66.9	42.3	49.1	51.2	58.2

Table 6: **Impact of Encoder Depth.** We evaluate the impact of increasing encoder depth. Our final evaluations use Encoder Depth = 12

Our ablation study 13 evaluates different loss function strategies for optimizing FRAME’s alignment with CLIP’s class token. We begin with a baseline Mean Squared Error (MSE) approach, which yields modest results (32.4% zero-shot accuracy on UCF-101 and 39.2% on HMDB-51). Switching to Cosine Embedding Loss substantially improves performance (55.4% and 48.1% zero-shot accuracy respectively) by directly optimizing for directional similarity between embedding vectors. Adding

¹<https://huggingface.co/docs/transformers/en/accelerate>

Number of Epochs	DAVIS	VIP	JHMDB	CamVid	HMDB-51	UCF-101
	$J \& F_m$	mIoU	PCK@0.1	mIoU	%	%
20	31.3	19.3	18.2	20.5	52.7	56.5
40	55.4	33.3	35.6	30.4	52.2	57.7
60	65.7	42.1	48.4	58.7	52.5	59.2
70	66.3	42.0	49.0	62.8	52.1	58.5
90	66.1	42.0	48.7	62.9	50.2	58.6
150	65.2	41.7	48.6	61.2	51.5	55.7

Table 7: **Impact of Number of Epochs.** We evaluate the effect of training for different numbers of epochs. Our final evaluations correspond to 70 epochs.

Kinetics (%)	DAVIS	VIP	JHMDB
	$J \& F_m$	mIoU	PCK@0.1
20%	55.7	36.8	41.6
30%	63.2	40.3	45.1
40%	65.6	41.2	48.7
70%	65.2	41.4	48.8
80%	65.3	41.0	48.5
100%	64.9	41.2	48.3

Table 8: **Impact of Dataset Size.** We evaluate the effect of varying the percentage of the Kinetics-400 dataset used for pretraining. Our final evaluations use 40% of the dataset.

Mean Scaling further enhances results (57.2% and 50.3%) by normalizing loss components to prevent one component from dominating the gradient updates, ensuring balanced learning across both semantic and spatial features. The combination of Cosine Embedding Loss with Mean Scaling and Cosine Annealing learning rate scheduling achieves the best performance (58.5% and 52.1%), as the warm restarts help escape local minima during optimization. Our exploration of techniques like Loss Dropout on top of the final version (temporarily disabling one loss component) don’t yield further improvements, suggesting our approach with cosine annealing already achieves near-optimal alignment between FRAME’s class token representations and CLIP’s semantic space. We have skipped including the variations in how well patch tokens align with DINO’s patch tokens, since the impact was minimal.

Broader Impact

This work introduces FRAME, a self-supervised video frame encoder that distills dense spatial and semantic features from pretrained image models, and augments them with lightweight temporal modeling to produce temporally consistent video representations. By leveraging existing image-based models (e.g., DINO, CLIP) rather than training from scratch on large-scale video datasets, our approach significantly reduces the computational cost and data requirements typically associated with video model training. The modular and efficient nature of FRAME promotes accessibility and scalability in domains where dense video prediction is valuable but labeled data is scarce—such as in education, scientific research, healthcare, and environmental monitoring. Additionally, by lowering the barrier to entry for high-quality video representation learning, our method may contribute to the broader democratization of video AI technologies.

However, since FRAME builds upon pretrained image models, it may inherit biases present in those foundation models. This can affect fairness, especially in downstream applications involving human-centric or safety-critical scenarios. Moreover, mispredictions—such as incorrect temporal alignment or false localization—could lead to cascading failures in safety-critical systems like autonomous navigation, medical video analysis, or security applications. To mitigate these risks, we encourage responsible deployment practices, including human-in-the-loop systems, clear documentation of limitations, and proactive auditing of downstream use cases. As a foundational model, the societal impact of FRAME will depend significantly on how it is integrated into applied systems.

Resolution	DAVIS	VIP	JHMDB	CamVid
	$J\&F_m$	mIoU	PCK@0.1	mIoU
224×224	63.5	38.5	48.5	61.0
320×320	64.5	40.0	48.5	62.1
400×400	66.3	42.0	49.0	62.8
512×512	66.5	42.5	49.0	62.8
720×720	66.5	42.0	49.0	62.7

Table 9: **Impact of Image Resolution.** We evaluate the effect of varying the input image resolution on performance across different datasets. Performance generally increases with resolution before plateauing at 512×512.

Number of Frames	DAVIS	VIP	JHMDB	CamVid	UCF101	HMDB101
	$J\&F_m$	mIoU	PCK@0.1	mIoU	mIoU	Accuracy
1	61.3	38.4	46.1	59.2	60.2	53.3
2	62.1	40.7	46.9	60.3	58.9	50.6
3	63.6	41.0	47.8	62.1	59.2	51.2
4	65.7	42.2	48.3	63.2	56.3	50.4
5	66.3	42.4	49.0	62.8	58.5	52.1
6	63.8	39.5	48.6	61.3	56.4	53.1
7	63.9	39.4	43.2	61.2	58.6	52.2

Table 10: **Impact of Number of Memory Frames.** We evaluate the effect of varying the number of past frames for memory on performance across different datasets. Performance generally peaks with 4-5 frames, then begins to decline with more frames, likely due to increased complexity of motion.

Pooled Region-Based Tracking. To evaluate the temporal consistency of FRAME features, we adopt a pooled region-based tracking approach inspired by prior region-centric pipelines [44, 25]. For each video frame, we extract spatially dense patch tokens using the FRAME encoder. We then apply an off-the-shelf segmentation model such as DINO-SAM [44] to generate region proposals. For each region, we compute a region-level feature by mean-pooling the FRAME patch tokens corresponding to the region’s mask. To propagate object identity across time, we perform nearest-neighbor matching of these pooled region features between consecutive frames using cosine similarity. Tracking is initialized from the annotated mask in the first frame by extracting its pooled feature and then iteratively matching it to regions in subsequent frames. Compared to patch-level correspondence, this region-centric formulation could be more robust to intra-object appearance variations and local noise. Moreover, FRAME features exhibit significantly better temporal consistency than DINO (as presented in the main paper Table 3), enabling more accurate region matching across frames (Fig. 7). We evaluate this tracking pipeline on DAVIS [33], measuring performance using the standard $J\&F_m$ metric. FRAME outperforms DINO variants in this setup, while being close to SAM 2[40].

Multi-Object Tracking via Region Pools. A key strength of this pooled region-based approach is its natural extension to *multi-object tracking*. Unlike models such as SAM2, which require iterative prompting or segmentation for each object in each frame—leading to high computational and memory overhead—our approach could potentially all objects simultaneously using pooled features derived from a single forward pass of FRAME. Specifically, we initialize pooled region embeddings for all masks in the annotated frame and independently propagate them forward through the video using per-region cosine similarity. This allows us to track multiple objects in parallel without re-encoding the video or repeatedly invoking a segmentation model. As a result, our method could enable efficient many-object tracking and segmentation at scale, making it especially suitable for long videos, memory-constrained settings, or applications involving dense object populations. We view this as a promising future direction for leveraging generic video encoders like FRAME for scalable open-world video object tracking.

Method	Backbone	Pre-training Dataset	DAVIS	VIP	JHMDB	CamVID
			$J \& F_m$	mIoU	PCK@0.1	mIoU
FRAME (encoder)	ViT S/16	Kinetics	65.7	41.2	48.7	62.1
FRAME (decoder)	ViT S/16	Kinetics	62.1	39.4	46.3	59.2
FRAME (encoder)	ViT S/16	Kinetics + Ego4D	66.3	42.0	49.0	62.4
FRAME (decoder)	ViT S/16	Kinetics + Ego4D	62.4	39.2	46.1	59.4
FRAME (encoder)	ViT S/16	Kinetics + Ego4D + SA-V	65.8	42.1	48.7	62.8
FRAME (decoder)	ViT S/16	Kinetics + Ego4D + SA-V	62.6	38.9	46.7	58.8

Table 11: **Impact of Encoder vs. Decoder Features in Model Performance.** We analyze the effect of encoder versus decoder features for evaluation. Across all pre-training settings, features extracted from the encoder consistently yield better performance than those from the decoder, highlighting the benefits of anticipation and memory in video understanding.

Teacher Net	DAVIS	VIP	JHMDB	CamVid (mIoU)		HMDB-51	UCF-101
			PCK@0.1	Current	Future	Accuracy	Accuracy
DINO+CLIP	74.4	48.2	64.3/86.0	62.6	54.0	76.1	69.7
DINO	74.1	48.1	64.4/86.0	62.5	54.1	56.4	52.7

Table 12: **Abalating the teacher network.** Comparison between DINO+CLIP and standalone DINO as teacher networks across multiple benchmarks.

C.1

Frame Delta Selection for Anticipation Decoders To determine appropriate frame offsets (*frame deltas*) for the semantic and spatial anticipation decoders in FRAME, we conducted an empirical analysis of feature variability across time. The goal was to select temporal distances that induce meaningful representation change—sufficient to enable predictive learning—without introducing excessive noise or instability due to long-term drift or scene discontinuities.

Setup. We evaluated temporal feature variability on a subset of 200 videos sampled from the Kinetics-400 [24], DAVIS [33] datasets. For each video, we extracted a sequence of frames and computed:

- Global features using CLIP’s ViT-B/32 class token.
- Local features using DINO’s ViT-S/16 patch tokens.

We then measured the feature change between frame F_t and F_{t+k} using cosine distance. For CLIP, we computed cosine distance between \mathbf{c}_{cls}^t and \mathbf{c}_{cls}^{t+k} ; for DINO, we averaged cosine distances between corresponding patch tokens across the frame.

Results. Our analysis reveal that CLIP global features exhibit relatively low temporal variation, with cosine distances increasing gradually across time and DINO patch features changed more rapidly, reflecting the fine-grained and localized nature of DINO representations.

Choice of Deltas. Based on this analysis, we selected a frame delta of 4 for the semantic anticipator (CLIP-like) and a delta of 2 for the spatial anticipator (DINO-like). These deltas were chosen to balance the temporal predictiveness of each target with the model’s learning capacity: they represent sufficient future context to encourage meaningful anticipation while avoiding overburdening the model with distant and unstable predictions. This design choice is further validated by downstream performance, where these deltas yield strong results across video segmentation and tracking tasks.

Method	UCF-101		HMDB-51	
	Zero-shot	Linear	Zero-shot	Linear
FRAME (MSE)	32.4	50.4	39.2	68.9
FRAME (Cosine Embedding Loss)	55.4	67.9	48.1	75.1
FRAME (Cosine + Mean Scaling)	57.2	68.8	50.3	75.6
FRAME (Cosine + Mean Scaling + Cosine Annealing)	58.5	69.7	52.1	76.1
FRAME (+ Loss Dropout)	58.3	69.9	51.9	75.8

Table 13: **Comparison of Loss Functions for Video Classification.** Performance of FRAME using different loss strategies when learning CLIP’s global semantic features (CLS token). .

Backbone	Dataset	DAVIS			VIP	JHMDB
		$J \& F_m$	J_m	F_m	mIoU	PCK@0.1 / PCK@0.2
ViT-S/16	Kinetics	65.7	62.1	69.2	41.2	48.7 / 79.2
ViT-S/16	Kinetics+Ego4D	66.3	62.9	69.8	42.0	49.0 / 79.3
ViT-S/16	Kinetics+Ego4D+SA-V	65.8	62.7	68.9	42.1	48.7 / 78.9
ViT-S/8	Kinetics	73.2	69.5	77.0	47.9	64.1 / 85.9
ViT-S/8	Kinetics+Ego4D	74.4	69.9	79.0	48.2	64.3 / 86.0
ViT-S/8	Kinetics+Ego4D+SA-V	74.2	69.7	79.0	48.4	64.2 / 86.0

Table 14: **Data Ablation Study for FRAME.** Performance comparison using different training datasets across ViT-S/16 and ViT-S/8 architectures.

Decoder Depth	DAVIS	VIP	JHMDB	CamVid	VSPW
	$J \& F_m$	mIoU	PCK@0.1	mIoU	mIoU
1	66.3	42.0	49.0	62.8	38.9
2	66.6	42.2	48.9	61.4	38.1
3	63.7	41.9	48.1	60.3	37.3
5	62.5	41.6	45.3	59.1	37.0

Table 15: **Impact of Decoder Depth.** Increasing the decoder depth beyond 2 layers degrades performance across all datasets. Our final model uses a shallow decoder with depth = 1.

Method	DAVIS	VIP	JHMDB	CamVid	VSPW
	$J \& F_m$	mIoU	PCK@0.1	mIoU	mIoU
FRAME (w/o memory)	62.6	39.2	46.7	60.1	37.3
FRAME (w/o anticipation)	65.5	41.2	48.6	62.3	38.0
FRAME (w/ memory + w/ anticipation)	66.3	42.0	49.0	62.8	38.9

Table 16: **Impact of Memory and Anticipation Components.** We evaluate the impact of memory and anticipation on FRAME performance across different datasets when pre-trained with Kinetics and Ego4d.

Model	Zero-Shot (%)		Linear (%)	
	HMDB-51	UCF-101	HMDB-51	UCF-101
CLIP ViT-L/14	55.9	60.6	78.1	71.3
FRAME ViT-S/16	55.1	58.5	76.1	71.1
FRAME ViT-B/16	55.7	59.6	78.5	72.2
FRAME ViT-L/14	55.3	59.9	76.3	71.6

Table 17: **Video Activity Classification Comparison.** We report zero-shot and linear classification accuracy on HMDB-51 and UCF-101. FRAME performs competitively with CLIP (ViT-L/14).

Model	CamVid (mIoU)	VSPW (mIoU)
PIDNet [56]	84.6	–
DVIS++ [58]	–	63.8
DINOv2 ViT-L/14	74.1	46.5
FRAME ViT-L/14	77.9	52.3

Table 18: **Semantic Segmentation Results.** FRAME approaches state-of-the-art performance (PIDNet [56] for CamVid and DVIS++ [58] for VSPW) using a simple U-Net decoder.

Dataset	License	Notes
DAVIS 2017	CC BY-NC-SA 4.0	Academic use only, non-commercial
Kinetics-400	DeepMind Terms of Use	Freely available for research
Ego4D	Ego4D Data Use Agreement	Requires signed agreement for access
UCF-101	Custom (UCF License)	Research only; redistribution prohibited
HMDB-51	Custom (HMDB License)	Academic and research use only
JHMDB	Follows HMDB terms	Derived from HMDB, same constraints
VIP (Video Instance Parsing)	CC BY-NC-SA 4.0	Research use, attribution required
CamVid	Custom (CamVid Terms)	Academic use with citation
VSPW	CC BY-NC-SA 4.0	Research permitted, commercial use restricted

Table 19: **Licensing Information for Datasets Used in Our Work.** All the datasets are standard academic datasets and are publicly available for academic research.

Training Set	DAVIS ($J \& F_m$)	VIP (mIoU)	JHMDB (PCK@0.1)	CamVid (mIoU)
Kinetics-400 (80K) + Ego4D Subset 1	66.1	42.3	48.7	62.4
Kinetics-400 (80K) + Ego4D Subset 2	66.4	42.1	48.9	63.0
Kinetics-400 (80K) + Ego4D Subset 3	66.0	42.2	48.7	62.7
Kinetics-400 (80K) + Ego4D Subset 4	65.8	42.0	48.5	62.5
Kinetics-400 (80K) + Ego4D (700 videos)	66.3	42.4	49.0	62.8
Full Kinetics-400 + Full Ego4D	66.5	42.6	48.9	63.1

Table 20: **Impact of Training Data Composition.** We compare FRAME performance when trained on various Ego4D subsets (combined with Kinetics-400). Subset results are stable, with minor variation across tasks. Final numbers reported in the paper use 80K Kinetics-400 videos and 700 Ego4D videos (highlighted in blue). Slight performance gains are observed with full-scale pretraining, while some subsets match or even exceed full training on specific tasks.

Model	Params (M)	DAVIS ($J \& F_m$)	VIP (mIoU)	JHMDB (PCK@0.1)
DINO ViT-S/16	21	61.8	36.2	45.6
FRAME ViT-S/16	38	66.3	42.0	49.0
DINO ViT-S/8	21	69.9	39.5	56.5
FRAME ViT-S/8	38	74.4	48.2	64.3
DINO ViT-B/16	85	63.2	39.1	48.2
FRAME ViT-B/16	101	68.2	42.7	49.4
DINO ViT-B/8	85	72.3	44.6	58.9
FRAME ViT-B/8	101	75.1	49.7	65.7
DINOv2 ViT-L/14	300	64.6	43.4	48.3
FRAME ViT-L/14	109	67.9	45.1	51.3

Table 21: **Model Scale, Runtime, and Performance Comparison.** We report parameter count and performance on DAVIS [33], VIP [59], and JHMDB [22] for DINO (v1/v2) and FRAME across various ViT backbones and patch sizes. FRAME consistently improves over the corresponding DINO baseline at each scale, and shows strong gains with smaller models like ViT-S/8. This highlights (1) the benefit of moving from ViT-S to ViT-B, (2) FRAME’s improvement over DINO at every patch resolution, and (3) a favorable accuracy-vs-compute trade-off for FRAME models.

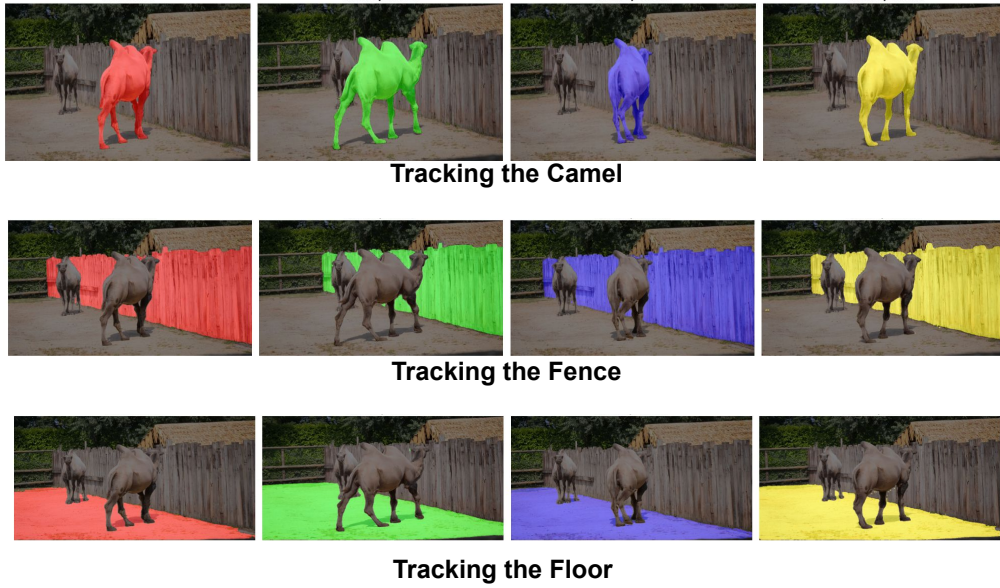


Figure 7: **Region-based tracking with FRAME.** We track different objects—eg. camel, fence, and floor—across time using FRAME-pooled region features. Each row shows the temporal propagation of a single object, demonstrating the ability of FRAME to support accurate and consistent tracking of diverse regions.